J Eng Math (2007) 57:351–363
DOI 10.1007/s10665-006-9060-3

ORIGINAL ARTICLE

Vibration analysis of a rotating flexible shaft–disk system

Molka Attia Hili · Tahar Fakhfakh · Mohamed Haddar

Received: 15 May 2005 / Accepted: 24 June 2006 / Published online: 13 September 2006

Abstract Free vibrations of a spinning disk–shaft system are analysed using the finite-element method. The spinning disk is described by the Kirchhoff plate theory. The shaft is modelled by a rotating beam. Using Lagrange's principle and including the rigid-body translation and tilting motion, equations of motion of the spinning flexible disk and shaft are derived consistently to satisfying the geometric compatibility conditions on the internal boundaries among the substructures. The finite-element method is then used to discretize the derived governing equations. The method is applied to the shaft–disk spinning system. The sensitivity to the running speed as well as the effect of both disk flexibility and boundary condition on the natural frequencies of the spinning system are numerically investigated.

Keywords Finite-element method · Natural frequencies · Sensistivity analysis · Spinning disk

1 Introduction

A spinning shaft–disk system (Fig. 1) serves as a model for many rotating systems such as circular saws, turbomachinery, rotors, etc. In these applications, the flexibility of the disk and the shaft may be important and one has to use a coupled vibration model that admits elastic deflection of both components.

Research on these and similar applications has generated large bodies of literature on the dynamics of spinning shafts and spinning disks in the absence of coupling. However, relatively little work has been done on coupled disk–shaft dynamics.

Chivens and Nelson [1] analytically obtained the natural frequencies and critical speed of an axisymmetric disk–spindle system coupled through a thin rigid clamp. They concluded that the disk flexibility changes

M. A. Hili · T. Fakhfakh · M. Haddar (✉)
Unit of Mechanics, Modelling and Production U2MP,
National school of Engineers of Sfax,
BP.W.3038 Sfax, Tunisia
e-mail: mohamed_haddar@yahoo.fr

M. A. Hili
e-mail: molka_hili@yahoo.fr

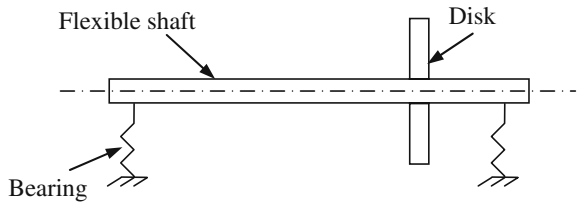

Fig. 1 Spinning system

the natural frequencies but has little effect on the critical speeds. Flowers and Ryan [2] and Flowers and Wu [3] examined coupled disk–spindle dynamics for turbomachinery applications. Jang et al. [4] carried out a free-vibration analysis of a spinning flexible disk–spindle system supported by a ball bearing and a flexible shaft using the finite-element method and substructure synthesis. Lee [5] and Lim [6] examined the coupled vibration of disk–spindles in the context of hard-disk drives. Parker [7] and Parker and Sathe [8] formulated the rotating-system problem in terms of extended operators that make the gyroscopic nature of the system evident. Shen and Ku [9] examined the related problem of vibration of multiple elastic disks mounted on a rigid spindle supported by flexible bearings.

In this paper, equations of motion for a spinning flexible disk including the rigid-body motion are derived by using the Kirchhoff theory and Lagrange's method. A finite-element method is used to discretize each component of the disk–shaft system. This method is used to investigate the influence of the flexibility of the disk on the natural frequencies of the system.

2 Equation of motion

Approximations of the governing equations of each component in the disk–shaft system are derived by using a finite-element method with consistent variables to satisfy the geometric compatibility conditions at internal interfaces. The motion of the rotating shaft can be described by the Euler beam. The motion of the spinning disk includes its rigid-body motion and its elastic deformation. Introducing the rigid-body motion of the spinning disk can satisfy the geometric compatibility between the disk and shaft interface.

2.1 Rotating-shaft equation of motion

The shaft is considered flexible. It is modelled by a beam with constant circular section and characterized by its kinetic and deformation energies. Its motion results from axial displacement and bending deformations in the xz- and yz-planes (Fig. 2).

The kinetic energy of the shaft is put in the following form [10]:

$$E_{ks} = \frac{\rho S}{2}\int_0^L \left(\dot{u}_x^2 + \dot{u}_y^2 + \dot{u}_z^2\right) \mathrm{d}z + \frac{\rho}{2} I \int_0^L \left(\dot{\theta}_x^2 + \dot{\theta}_y^2\right) \mathrm{d}z + 2\rho I \Omega \int_0^L \left(\dot{\theta}_x \theta_y\right) \mathrm{d}z + \rho I L \Omega^2, \tag{1}$$

where u_x, u_y are the bending displacements in the x- and y-directions, and u_z the axial displacement in the z-direction; θ_x and θ_y are small angles twist rotations around the x- and y-directions. Further ρ, S, L and I are the density, cross-sectional area, length and area moment of inertia of a shaft, respectively, and Ω is the shaft running speed.

The deformation energy of a rotating shaft is expressed as follows [10]:

$$E_{ds} = \frac{1}{2}\int_0^L ES\left(\frac{\partial u_z}{\partial z}\right)^2 \mathrm{d}z + \frac{1}{2}\int_0^L EI\left(\left(\frac{\partial \theta_x}{\partial z}\right)^2 + \left(\frac{\partial \theta_y}{\partial z}\right)^2\right) \mathrm{d}z, \tag{2}$$

where E is young's modulus of shaft.

Fig. 2 Rotating shaft

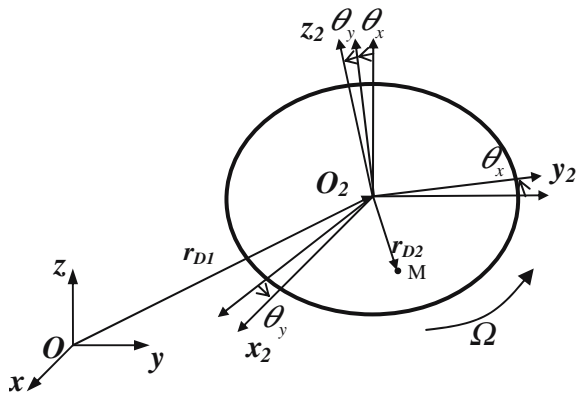

Fig. 3 Rotating flexible disk with rigid-body motion

The finite element used to discretize the shaft consists of a beam element of two nodes; the nodal displacement vector includes: four lateral displacements, four bending rotation angles (slopes) and two axial displacements. Its expression is:

$$\delta = \left[u_{x1},\ u_{y1},\ u_{z1},\ \theta_{x1},\ \theta_{y1},\ u_{x2},\ u_{y2},\ u_{z2},\ \theta_{x2},\ \theta_{y2}\right]^{\mathrm{T}}, \tag{3}$$

The displacements and the slopes along the shaft elements are represented by shape functions as follows:

$$\begin{Bmatrix} u_x \\ u_y \\ u_z \end{Bmatrix} = [N]\{\delta\}, \tag{4}$$

and

$$\begin{Bmatrix} \theta_x \\ \theta_y \end{Bmatrix} = \begin{Bmatrix} -\dfrac{\partial u_y}{\partial z} \\ \dfrac{\partial u_x}{\partial z} \end{Bmatrix} = \begin{bmatrix} -1 & 0 \\ 0 & 1 \end{bmatrix} [D]\{\delta\}, \tag{5}$$

where $[N]$ is the matrix of shape functions [10]:

$$[N] = \begin{bmatrix} \beta_1 & 0 & 0 & 0 & \gamma_1 & \beta_2 & 0 & 0 & 0 & \gamma_2 \\ 0 & \beta_1 & 0 & -\gamma_1 & 0 & 0 & \beta_2 & 0 & -\gamma_2 & 0 \\ 0 & 0 & \alpha_1 & 0 & 0 & 0 & 0 & \alpha_2 & 0 & 0 \end{bmatrix}, \tag{6}$$

β_i, and γ_i are the typical displacement functions of a beam in bending:

$$\beta_1\ (z) = 1 - \frac{3z^2}{L^2} + \frac{2z^3}{L^3}, \quad \beta_2\ (z) = \frac{3z^2}{L^2} - \frac{2z^3}{L^3}, \tag{7, 8}$$

$$\gamma_1\ (z) = -z + \frac{2z^2}{L} - \frac{z^3}{L^2}, \quad \gamma_2\ (z) = -\frac{z^2}{L} + \frac{z^3}{L^2}; \tag{9, 10}$$

further α_i are the typical displacement functions of a beam in traction-compression:

$$\alpha_1 = 1 - \frac{z}{L}, \quad \alpha_2 = \frac{z}{L}, \tag{11, 12}$$

$$\text{and } [D] = \frac{\partial}{\partial z}\begin{bmatrix} \beta_1 & 0 & 0 & 0 & \gamma_1 & \beta_2 & 0 & 0 & 0 & \gamma_2 \\ 0 & \beta_1 & 0 & -\gamma_1 & 0 & 0 & \beta_2 & 0 & -\gamma_2 & 0 \end{bmatrix}, \tag{13}$$

Upon substitution Eqs. 4 and 5 in the expressions (1), (2), Lagrange's equations provide the equation of motion of the shaft:

$$[M_S]\ \left\{\ddot{\delta}\right\} + \Omega\ [G_S]\ \left\{\dot{\delta}\right\} + [K_S]\ \{\delta\} = \{0\}, \tag{14}$$

where $[M_S], [G_S]$ and $[K_S]$ are, respectively, mass, gyroscopic and stiffness matrices of the shaft which may be expressed as:

$$[M_S] = \rho S \int_0^L [N]^{\mathrm{T}}\,[N]\,\mathrm{d}z + \rho I \int_0^L [D]^{\mathrm{T}}\,[D]\,\mathrm{d}z, \tag{15}$$

$$[G_S] = \rho I \int_0^L [D]^{\mathrm{T}} \begin{bmatrix} 0 & -1 \\ 1 & 0 \end{bmatrix} [D]\,\mathrm{d}z, \tag{16}$$

$$[K_A] = EI \int_0^L [B]^{\mathrm{T}}\,[B]\,\mathrm{d}z, \tag{17}$$

with

$$[B] = \frac{\partial^2}{\partial z^2}\,[N]\,. \tag{18}$$

2.2 Rotating-disk equation of motion

Figure 3 shows a spinning flexible disk with a constant angular speed Ω, and undergoing an infinitesimal rigid-body motion as well as an elastic deformation. The local reference frame, $R_2(O_2, x_2, y_2, z_2)$ is located at the centre of the disk after it has undergone the infinitesimal rigid body translation (X_D, Y_D, Z_D) and tilting motion (θ_x, θ_y) with respect to the inertial reference frame $R(O, x, y, z)$; the elastic deformation of the disk is observed with respect to the local reference frame $R_2(x_2, y_2, z_2)$.

The displacements due to elastic deformation are expressed by the Kirchhoff plate theory as follows [11, Chapter 4],

$$U = \begin{Bmatrix} u(x,y,z,t) = z\dfrac{\partial\, w\,(x,y,t)}{\partial x} \\ v\,(x,y,z,t) = z\dfrac{\partial\, w\,(x,y,t)}{\partial y} \\ w(x,y,z) = w\,(x,y,t) \end{Bmatrix}, \tag{19}$$

where w is the displacement in the z-direction in the middle plane of a disk.

In Fig. 3, the position vector of a point M in the disk is expressed as follows:

$$\overrightarrow{OM} = \vec{r}_{D1} + \vec{r}_{D2}, \tag{20}$$

where $\vec{r}_{D1}$ is the position vector in the inertial reference frame to the origin of the local reference frame and $\vec{r}_{D2}$ is the position vector of a point in the disk with respect to the local reference frame. They can be expressed as follows:

$$\vec{r}_{D1} = X_D\,\vec{x} + Y_D\,\vec{y} + Z_D\,\vec{z}, \tag{21}$$

$$\vec{r}_{D2} = \left[(x+u)\cos\theta + (y+v)\sin\theta\right]\vec{x}_2 + \left[(x+u)\sin\theta + (y+v)\cos\theta\right]\vec{y}_2 + w\,\vec{z}_2, \tag{22}$$

where $\theta = \Omega t$, and x, y are the distance in the x- and y-directions from the centre of a disk to a point before elastic deformation. The velocity of the point M in the disk $\vec{V}_D$ can be written as the time derivative of the position vector,

$$\vec{V}_D = \frac{\mathrm{d}\overrightarrow{OM}}{\mathrm{d}t}. \tag{23}$$

The kinetic energy of the disk considered as thin can be expressed as follows:

$$E_{kD} = \frac{1}{2}\rho_D\, h \int_A \vec{V}_D \vec{V}_D \mathrm{d}A, \tag{24}$$

where ρ_D and h are the density and thickness of the disk, respectively, and A is its area.

The deformation energy of the disk can be expressed as follows [11, Formula 4.2.55]:

$$E_{DD} = \frac{1}{2}\int_A \{\chi\}^{\mathrm{T}}[H_f]\{\chi\}\mathrm{d}A, \tag{25}$$

where, $\{\chi\}$ is the curvature vector [11, Formula 4.2.55]:

$$\{\chi\}^{\mathrm{T}} = -\left\{\frac{\partial^2 w}{\partial x^2} \quad \frac{\partial^2 w}{\partial y^2} \quad 2\frac{\partial^2 w}{\partial y \partial x}\right\}^{\mathrm{T}}, \tag{26}$$

$\left[H_f\right]$ is the elasticity matrix due to bending motion [11, Formula 4.2.4]:

$$\left[H_f\right] = \frac{E h^3}{12\left(1-\nu^2\right)}\begin{bmatrix} 1 & \nu & 0 \\ \nu & 1 & 0 \\ 0 & 0 & \frac{1-\nu}{2} \end{bmatrix}, \tag{27}$$

E and ν are Young's modulus and the Poisson ratio.

Applying Lagrange's principle with Eqs. 24 and 25, results in six nonlinear equations of the spinning disk under the coupled rigid-body motion and elastic deformation. Under the assumption of infinitesimal rigid-body motion, the derived equations can be linearized with respect to θ_x, and θ_y as follows:

$$\rho_D h\,\ddot{X}_D = 0, \tag{28}$$

$$\rho_D h\ddot{Y}_D = 0, \tag{29}$$

$$\rho_D h\left(\ddot{Z}_D + \ddot{w}\right) = 0, \tag{30}$$

$$\rho_D h\begin{pmatrix} \ddot{\theta}_x x^2 \sin^2\theta + \ddot{\theta}_x y^2\cos^2\theta + x^2\Omega\dot{\theta}_y + y^2\Omega\dot{\theta}_y \\ +wx\Omega^2\sin\theta + wy\Omega^2\cos\theta + \ddot{w}x\sin\theta + \ddot{w}y\cos\theta \end{pmatrix} = 0, \tag{31}$$

$$\rho_D h\begin{pmatrix} \ddot{\theta}_y x^2 \cos^2\theta + \ddot{\theta}_y y^2\sin^2\theta + x^2\Omega\dot{\theta}_x + y^2\Omega\dot{\theta}_x \\ -wx\Omega^2\cos\theta + wy\Omega^2\sin\theta - \ddot{w}x\cos\theta + \ddot{w}y\sin\theta \end{pmatrix} = 0, \tag{32}$$

$$\begin{aligned} &\rho h\left(\ddot{\theta}_x\left(x\sin\theta + y\cos\theta\right) + \ddot{\theta}_y\left(y\sin\theta - x\cos\theta\right) + 2\dot{\theta}_x\Omega\left(x\cos\theta - y\sin\theta\right) + 2\dot{\theta}_y\Omega\left(y\cos\theta + x\sin\theta\right)\right) \\ &\quad + \rho h\left(\ddot{Z}_D + \ddot{w}\right) - \frac{\partial^2 M_x}{\partial x^2} - \frac{\partial^2 M_y}{\partial y^2} - 2\frac{\partial^2 M_{xy}}{\partial xy} = 0, \end{aligned} \tag{33}$$

where $M_i\,(i = x, y, z)$ are the internal moments in the middle plane of a disk and they are defined as follows[11, Chapter 4]:

$$M_x = -\frac{E h^3}{12\left(1-\nu^2\right)}\left(\frac{\partial^2 w}{\partial x^z} + \nu\frac{\partial^2 w}{\partial y^2}\right), \tag{34}$$

$$M_y = -\frac{E h^3}{12\left(1-\nu^2\right)}\left(\nu\frac{\partial^2 w}{\partial x^2} + \frac{\partial^2 w}{\partial y^2}\right), \tag{35}$$

$$M_{xy} = \frac{E h^3}{12\left(1+\nu\right)}\frac{\partial^2 w}{\partial y \partial x}, \tag{36}$$

The weak form of Eqs. 28–33 of the disk is expressed as follows:

$$\begin{aligned} &\begin{Bmatrix} X \\ Y \\ Z \\ \theta_X \\ \theta_Y \end{Bmatrix}^{\mathrm{T}}\begin{bmatrix} M_D & 0 & 0 & 0 & 0 \\ 0 & M_D & 0 & 0 & 0 \\ 0 & 0 & M_D & 0 & 0 \\ 0 & 0 & 0 & I_D & 0 \\ 0 & 0 & 0 & 0 & I_D \end{bmatrix}\begin{Bmatrix} \ddot{X}_D \\ \ddot{Y}_D \\ \ddot{Z}_D \\ \ddot{\theta}_X \\ \ddot{\theta}_y \end{Bmatrix} + \Omega\begin{Bmatrix} \theta_X \\ \theta_Y \end{Bmatrix}^{\mathrm{T}}\begin{bmatrix} 0 & 2I_D \\ -2I_D & 0 \end{bmatrix}\begin{Bmatrix} \dot{\theta}_x \\ \dot{\theta}_y \end{Bmatrix} \\ &\quad + \int_A \begin{Bmatrix} Z \\ W \end{Bmatrix}^{\mathrm{T}}\begin{bmatrix} 0 & \rho_D h \\ \rho_D h & 0 \end{bmatrix}\begin{Bmatrix} \ddot{Z}_D \\ \ddot{w}_D \end{Bmatrix}\mathrm{d}A \end{aligned}$$

$$+\rho_D h\int_A \begin{Bmatrix}\theta_X\\ \theta_Y\\ W\end{Bmatrix}^{\mathrm{T}} \begin{bmatrix}0 & 0 & x\sin\theta+y\cos\theta\\ 0 & 0 & y\sin\theta-x\cos\theta\\ x\sin\theta+y\cos\theta & y\sin\theta-x\cos\theta & 0\end{bmatrix} \begin{Bmatrix}\ddot{\theta}_x\\ \ddot{\theta}_y\\ \ddot{w}_D\end{Bmatrix} \mathrm{d}A$$

$$+2\rho_D h\,\Omega\int_A \begin{Bmatrix}\theta_X\\ \theta_Y\\ W\end{Bmatrix}^{\mathrm{T}} \begin{bmatrix}0 & 0 & y\sin\theta-x\cos\theta\\ 0 & 0 & -(x\sin\theta+y\cos\theta)\\ x\cos\theta-y\sin\theta & x\sin\theta+y\cos\theta & 0\end{bmatrix} \begin{Bmatrix}\dot{\theta}_x\\ \dot{\theta}_y\\ \dot{w}_D\end{Bmatrix} \mathrm{d}A$$

$$+\rho_D h\int_A W\ddot{w}_D\mathrm{d}A+2\rho_D h\,\Omega\int_A\left[\left(y\dot{w}\frac{\partial W}{\partial x}-x\dot{w}\frac{\partial W}{\partial y}\right)\right]\mathrm{d}A$$

$$-\rho_D\,h\,\Omega^2\int_A y^2\frac{\partial W}{\partial x}\frac{\partial w}{\partial x}+x^2\frac{\partial W}{\partial y}\frac{\partial w}{\partial y}\mathrm{d}A$$

$$+\frac{1}{2}\int_A\{\chi\}^{\mathrm{T}}[H_f]\{\chi\}\,\mathrm{d}A=0. \tag{37}$$

The finite element used to discretize the disk consists of a triangular element with three nodes (DKT elements). It is appropriate to analyze the circular disk and it gives satisfactory solutions with a small number of elements. The shape function of the transverse displacement uses a conforming Kirchhoff interpolation function$\langle N^w\rangle$ [11]:

$$w=\langle N^w\rangle\{\delta_D\}, \tag{38}$$

where $\delta_D=\left[w_1,\ \beta_{x1},\ \beta_{y1},\ w_2,\ \beta_{x2},\ \beta_{y2},\ w_3,\ \beta_{x3},\ \beta_{y3}\right]^{\mathrm{T}}$ is the nodal displacement vector.

$$\beta_{xi}=-\frac{\partial w_i}{\partial x},\quad \beta_{yi}=-\frac{\partial w_i}{\partial y},\quad i=1,3 \tag{39, 40}$$

The following element matrix equations of the disk can be obtained after substituting Eq. 38 in Eq. 37: $\left[M_D^R\right]$ is the inertia matrix corresponding to the rigid-body motions:

$$\left[M_D^R\right]=\begin{bmatrix}M_D & 0 & 0 & 0 & 0\\ 0 & M_D & 0 & 0 & 0\\ 0 & 0 & M_D & 0 & 0\\ 0 & 0 & 0 & I_D & 0\\ 0 & 0 & 0 & 0 & I_D\end{bmatrix}, \tag{41}$$

where M_D and I_D are the disk mass and mass moment of inertia, respectively. $\left[G_D^R\right]$ is the element gyroscopic matrix corresponding to the rigid-body tilting (θ_x, θ_y):

$$\left[G_D^R\right]=\begin{bmatrix}0 & 2I_D\\ -2I_D & 0\end{bmatrix}, \tag{42}$$

while $\left[M_{D1}^{RF}\right]$ is the element mass matrix coupled with the axial rigid translation and transverse displacement:

$$\left[M_{D1}^{RF}\right]=\rho_D h\int_{\Sigma^e}\langle N^w\rangle\mathrm{d}\Sigma \tag{43}$$

and $\left[M_{D2}^{RF}\right]$ is the element mass matrix coupled with the rigid-body tilting and transverse displacement.

$$\text{Further }\left[M_{D2}^{RF}\right]=\rho_D h\int_{\Sigma^e}\begin{Bmatrix}x\sin\theta+y\cos\theta\\ y\sin\theta-x\cos\theta\\ 0\end{Bmatrix}\langle N^w\rangle\mathrm{d}\Sigma, \tag{44}$$

while $\left[G_D^{RF}\right]$ is the element gyroscopic matrix coupled with the rigid-body tilting and transverse displacement defined by

$$\left[G_D^{RF}\right]=2\rho_D h\int_{\Sigma^e}\begin{Bmatrix}y\sin\theta-x\cos\theta\\ -(x\sin\theta+y\cos\theta)\\ 0\end{Bmatrix}\langle N^w\rangle\mathrm{d}\Sigma, \tag{45}$$

$\left[M_D^F\right]$ is the element mass matrix due to the transverse displacement:

$$\left[M_D^F\right] = \rho_D h \int_{\Sigma^e} \{N^w\} \langle N^w \rangle \mathrm{d}\Sigma, \tag{46}$$

$\left[G_D^F\right]$ is the element gyroscopic matrix due to the transverse displacement:

$$\left[G_D^F\right] = \rho_D\, h \int_{\Sigma^e} \left(y \{N^w\} \left\langle \frac{\partial N^w}{\partial x} \right\rangle - x \{N^w\} \left\langle \frac{\partial N^w}{\partial y} \right\rangle \right) \mathrm{d}\Sigma, \tag{47}$$

$\left[N_D^F\right]$ is the centrifuge effect matrices due to the transverse displacement:

$$\left[N_D^F\right] = \rho_D\, h \int_{\Sigma^e} \left(y^2 \left\{ \frac{\partial N^w}{\partial x} \right\} \left\langle \frac{\partial N^w}{\partial x} \right\rangle + x^2 \left\{ \frac{\partial N^w}{\partial y} \right\} \left\langle \frac{\partial N^w}{\partial y} \right\rangle \right) \mathrm{d}\Sigma, \tag{48}$$

$\left[K_D^F\right]$ is the element stiffness matrix due to the transverse displacement:

$$\left[K_D^F\right] = \int_{\Sigma^e} \langle \chi \rangle \left[H_f\right] \{\chi\} \mathrm{d}\Sigma, \tag{49}$$

Then the equation of motion of a spinning disk can be obtained:

$$[M_D] \left\{\ddot{\delta}_D\right\} + \Omega [G_D] \left\{\dot{\delta}_D\right\} + \left(\left[K_D^F\right] - \Omega^2 \left[N_D^F\right] \right) \{\delta_D\} = \{0\}, \tag{50}$$

where $[M_D]$ is the mass matrix:

$$[M_D] = \begin{bmatrix} \left[M_D^F\right] & \left[M_D^{RF}\right] \\ \left[M_D^{RF}\right] & \left[M_D^R\right] \end{bmatrix}, \tag{51}$$

$[G_D]$ is gyroscopic matrix (skew-symmetric):

$$[G_D] = \begin{bmatrix} \left[G_D^F\right] & \left[G_D^{RF}\right] \\ -\left[G_D^{RF}\right] & \left[G_D^R\right] \end{bmatrix}, \tag{52}$$

$\{\delta_D\}$, $\left\{\dot{\delta}_D\right\}$ and $\left\{\ddot{\delta}_D\right\}$ are, respectively, nodal disk displacement, velocity and acceleration vectors.

2.3 Global equation of motion

The element matrix equations derived in the previous sections are used with the geometric compatibility in the internal boundaries taken into account: (node where the disk is connected to the shaft (Fig. 1)):

$$X_D = u_x^c, \quad Y_D = u_y^c, \quad Z_D = u_z^c, \tag{53}$$

$$\theta_x = -\frac{\partial u_y^c}{\partial z}, \quad \theta_y = -\frac{\partial u_x^c}{\partial z}. \tag{54}$$

where superscript c denotes the deformation of the shaft at which the disk is connected.

Then, the matrix-vector equation of the entire shaft–disk system (Fig. 1) can be expressed as follows:

$$[M_T] \left\{\ddot{\delta}\right\} + \Omega [G_T] \left\{\dot{\delta}\right\} + \left([K_T] - \Omega^2 [N_T] \right) \{\delta\} = \{0\}. \tag{55}$$

where $[M_T]$, $[G_T]$, $[K_T]$ and $[C_T]$ are, respectively, global mass, gyroscopic, stiffness and centrifuge matrices; $\{\delta\}$, $\left\{\dot{\delta}\right\}$ and $\left\{\ddot{\delta}\right\}$ are, respectively, global nodal displacement, velocity and acceleration vectors.

3 Sensitivity of a disk–shaft system to the running speed

In high-speed applications (e.g., aircraft engines), gyroscopic effects may significantly alter a system's stability and dynamic behaviour. Eigenvalue derivatives evaluated for $\Omega = 0$ are calculated to assess the influence of the operating speed on the natural frequency spectrum. The associated eigenvalue problem of Eq. 55 is obtained from the separable solution $q = \phi_i e^{j\omega_i t}$:

$$\left\{-\omega_i^2\ [M_T] + j\,\Omega\ [G_T]\ \omega_i^+ \left([K_T] - \Omega^2\,[N_T]\right)\right\}\phi_i = 0. \tag{56}$$

The eigensensitivity analysis [12] calculates the natural frequency and vibration-mode derivatives with respect to the operating speed. When it is assumed that a zero-speed natural frequency ω_i has multiplicity m and arbitrarily chosen independent eigenvectors are $\Gamma = \langle\gamma_1, \ldots, \gamma_m\rangle^{\mathrm{T}}$ with normalization $\Gamma^{\mathrm{T}}\,[M_T]\,\Gamma = I_{m\times m}$, differentiation of Eq. 56 with respect to Ω yields:

$$\left(\left[\tilde{K}_T\right] - \omega_i^2\ [M_T] + \mathrm{j}\ \Omega\,[G_T]\ \omega_i\right)\phi_i' + \left(-2\omega_i\omega_i'\,[M_T] + \mathrm{j}\omega_i\,[G_T] + \mathrm{j}\ \Omega\,[G_T]\,\omega_i'\right)\phi_i = 0, \tag{57}$$

where

$$\left[\tilde{K}_T\right] = [K_T] - \Omega^2\,[N_T]\,. \tag{58}$$

Evaluation of Eq. 58 at $\Omega = 0$ yields:

$$\left([K_T] - \omega_i^2\ [M_T]\right)\phi_i' = \left(2\omega_i\omega_i'\,[M_T] - \mathrm{j}\omega_i\,[G_T]\right)\phi_i. \tag{59}$$

Note that ϕ_i can be written as a linear combination of eigenvectors Γ:

$$\phi_i = \Gamma\,a_i \tag{60}$$

where the a_i are uniquely obtained with the normalization $a_i^{\mathrm{T}}a_i = 1$.

From

$$h = \left(2\omega_i\omega_i'\,[M_T] - \mathrm{j}\omega_i\,[G_T]\right)\Gamma\,a_i, \tag{61}$$

the m solvability conditions $\gamma_1 h = \cdots = \gamma_m h = 0$ of the equation yield the symmetric $m \times m$ Hermitian eigenvalue problem,

$$Da_i = \omega_i' a_i, \tag{62}$$

$$\text{where } D = \frac{1}{2}\mathrm{j}\ \Gamma^{\mathrm{T}}\,[G_T]\ \Gamma. \tag{63}$$

The natural-frequency sensitivities ω_i' are obtained from the eigenvalues of Eq. 62.

For distinct modes at $\Omega = 0$, Eq. 62 becomes a scalar equation. Hence $\omega_i' = 0$ because $\gamma_i^{\mathrm{T}}\,[G_T]\ \gamma_i = 0$ for real γ_i and skew-symmetric $[G_T]$. The result $\omega_i' = 0$ indicates the natural frequencies of these modes are hardly affected by the operating speed.

For modes having a multiplicity $m = 2$ at $\Omega = 0$:

$$\Gamma = \langle\gamma_1, \gamma_2\rangle^{\mathrm{T}}, \tag{64}$$

D can be written as:

$$D = \begin{bmatrix} 0 & \gamma_1^{\mathrm{T}}\ [G_T]\ \gamma_2 \\ -\gamma_1^{\mathrm{T}}\ [G_T]\ \gamma_2 & 0 \end{bmatrix} \tag{65}$$

and its eigenvalues are:

$$\omega_{1,2}' = \pm\gamma_1^{\mathrm{T}}\,[G_T]\ \gamma_2/2. \tag{66}$$

This expression yields eigensolution approximations according to,

$$\omega_i - \omega_{i0} = (\Omega - \ \Omega_0)\,\omega_i'. \tag{67}$$

For $\Omega_0 = 0$ and ω_{i0} the corresponding eigenvalue, we get,

$$\omega_i = \omega_{i0} + \Omega\ \omega_i'. \tag{68}$$

According to Eq. 68, the degenerate zero-speed mode natural frequencies split into distinct ones as the operating speed increases.

4 Numerical results

To obtain the system's natural frequencies, the equation of motion of a global disk–shaft system (Eq. 55) is transformed to the state space matrix-vector equation, and the associated eigenvalue problem is solved. A computer program written in MATLAB, the organization chart of which is presented in Fig. 4, is developed to analyze the natural frequencies of a disk–shaft system as shown in Fig. 1.

4.1 Validation

In order to validate the developed calculation, the obtained natural frequencies of a single spinning disk (Fig. 5), with fixed boundary condition at its inner radius and undergoing the infinitesimal rigid-body motion as well as an elastic deformation, are compared with those found by Jang et al. [4] (Table 1). The disk has an outer diameter of 47·5 mm, an inner diameter of 15 mm and a thickness of 0·8 mm. It is made of aluminium.

Simulation results agree with those found by Jang and Lee within an 8% error.

4.2 Coupled vibration mode in a disk–shaft system

The studied disk–shaft is showed in Fig. 1. The shaft has a length of $L = 300$ mm and a diameter of 10 mm with simply supported boundary condition at the two extremities. A disk of 100 mm in diameter and 3 mm in thickness is mounted on the shaft at 75% of the shaft length. Both disk and shaft are made of steel. Figure 6 shows the finite-element model of the studied system. The disk is divided into

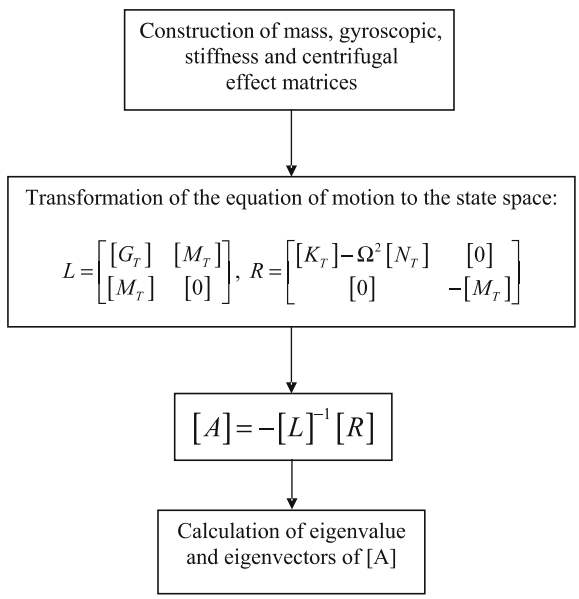

Fig. 4 Organization chart of developed computer program

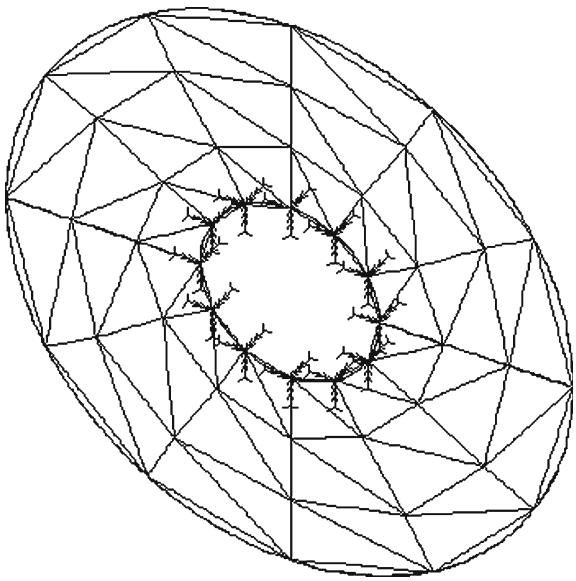

Fig. 5 A spinning disk

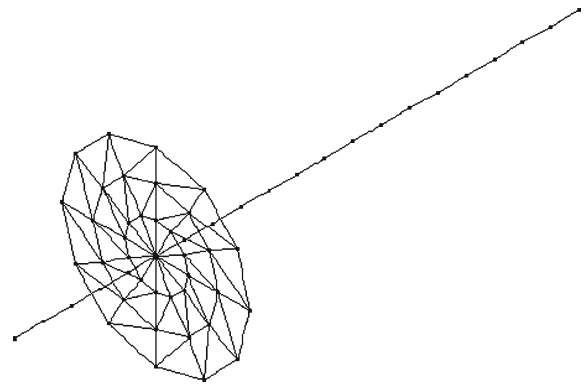

Fig. 6 Finite-element model of a disk–shaft system

Table 1 Comparison between simulated results and those found by Jang et al. [4]

Mode	Simulated results		Natural frequencies found by Jang et al. [4]	
	$\Omega = 0$	$\Omega = 5000$ rpm	$\Omega = 0$	$\Omega = 5000$ rpm
1	646 Hz	716 Hz	625 Hz	710 Hz
	646 Hz	551 Hz	625 Hz	547 Hz
2	658 Hz	601 Hz	633 Hz	630 Hz
3	746 Hz	884 Hz	740 Hz	902 Hz
	746 Hz	649 Hz	740 Hz	600 Hz

60 triangular elements ((3×4) in the radial and circumferential directions, respectively) and it has 171 degrees of freedom. The shaft is divided into 20 beam elements, and it has 100 degrees of freedom. Indeed, Figure 7 shows that convergence of the eigenvalues starts from a number of elements equal to 80.

Figure 8 shows the natural frequencies of a spinning system with flexible disk according the rotational speed. There are four families of vibration modes:

(i) Shaft bending modes: the associated natural frequencies depend on the shaft rotation speed and divide in two branches associated to the forward and backward whirl. This separation is due to gyroscopic effects (the gyroscopic matrix is skew-symmetric) and is confirmed by the sensitivity analysis presented in Sect. 3.

(ii) Coupled modes: these are the coupled modes between the disk and shaft. They can be clearly explained by the vibration-mode shape (Fig. 9). The first coupled mode is an axial vibration mode coupled with the transverse displacement of the disk and axial motion of the shaft; it can be also predicted and explained by the coupled governing equation of the disk in Eq. 30. The second coupled mode is a rocking vibration mode coupled with the transverse displacement of the disk and tilting motion of a shaft; it can be predicted and explained by the coupled governing equation of the disk in Eqs. 31 and 32.

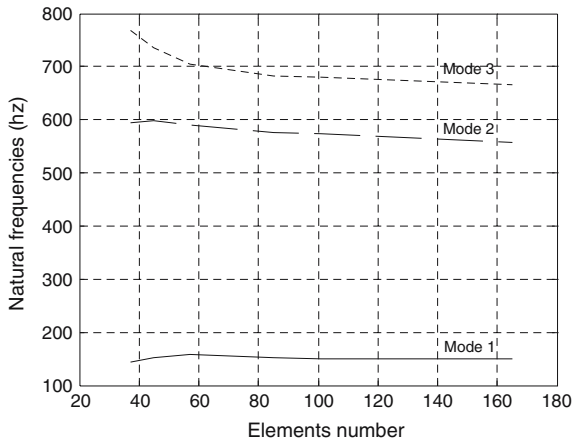

Fig. 7 Convergence test

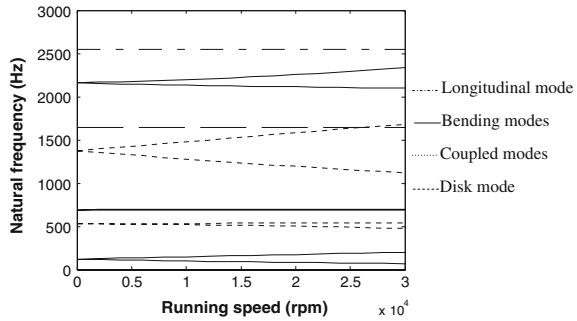

Fig. 8 Natural frequencies of a spinning disk–shaft system

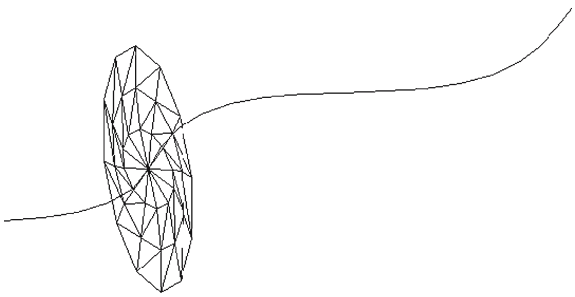

Fig. 9 Deformed shape of the second coupled mode (5000 rpm)

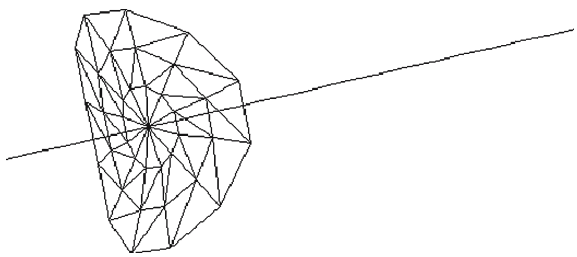

Fig. 10 Deformed shape of the disk mode (5000 rpm)

(iii) Disk modes: these are independent of the running speed and cannot be separated in two branches although they are double modes. The associated deformed shape (Fig. 10) shows that only the disk is affected.
(iv) Longitudinal mode which is a distinct mode that is independent of the running speed.

4.3 Influence of disk flexibility

Figure 11 shows the variation of the system's natural frequencies according to the running speed for two cases: (a) system with a rigid disk and (b) system with a flexible disk.

Only two families of vibration modes are obtained for the case of a system with a rigid disk: shaft-bending modes which are affected by disk mass and longitudinal mode. It should be noted that both shaft-bending modes and longitudinal mode are independent of disk flexibility. Therefore, disk flexibility changes the vibrational behaviour of the shaft–disk system.

4.4 Influence of boundary condition

The natural frequencies of the studied system were calculated for different types of boundary conditions: the shaft is simply supported, clamped and supported by elastic bearings at its extremities (bearing

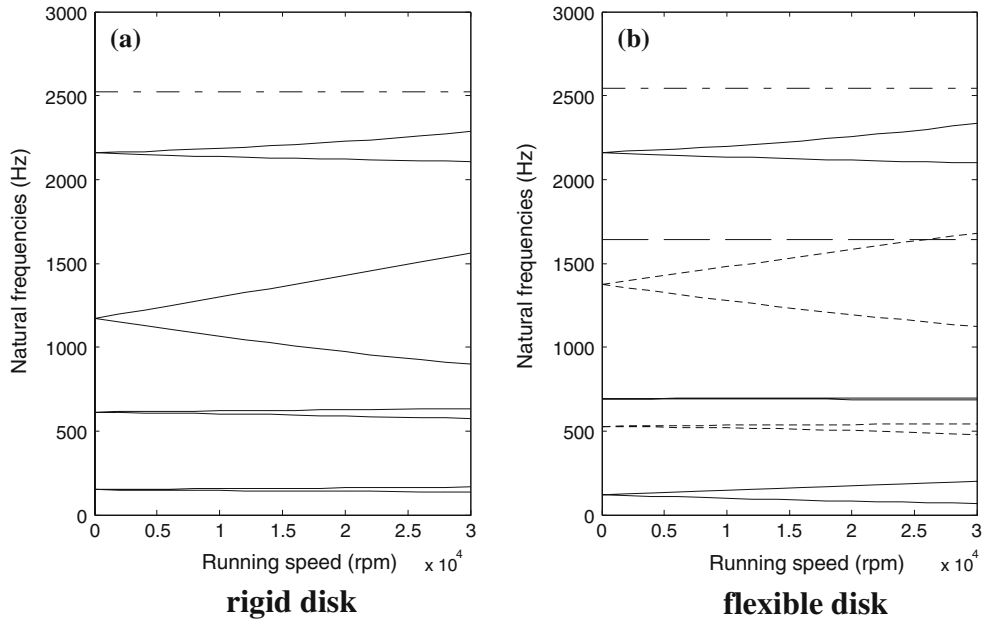

Fig. 11 Natural frequencies of a spinning disk–shaft system. (**a**) rigid disk. (**b**) flexible disk (· · ·· · · Longitudinal mode, —— Bending modes, ····· Coupled modes, - - - - - - Disk mode)

stiffness $k_{xx} = k_{yy} = 5{\cdot}510^5$ N/m, $k_{xy} = k_{xy} = 0$). Table 2 presents the obtained results for a system at rest ($\Omega = 0$).

The clamped boundary condition for the two studied cases causes an increase of natural frequencies. Inversely, the introduction of an elastic bearing decreases on the one hand the natural frequencies and on the other adds supplementary modes.

5 Conclusion

The equations of motion for a flexible spinning disk–shaft system including infinitesimal rigid-body motion as well as elastic deformation for describing disk motion have been derived by a finite-element method.The system's natural frequencies were calculated for different cases and the obtained results show that:

Table 2 Natural frequencies in Hertz for different boundary conditions

Modes	Rigid disk			Flexible disk		
	Simply supported	Clamped	Elastic bearing	Simply supported	Clamped	Elastic bearing
1	151	346	132	122	277	107
	151	346	132	122	277	107
2	612	915	431	528	652	383
	612	915	431	528	652	383
3	1174	1400	768	692	887	597
	1174	1400	768	692	887	597
4	2157	2597	1278	1375	1563	982
	2157	2597	1278	1375	1563	982

(i) The impact of gyroscopic effects is estimated by the natural-frequency sensitivity to the operating speed. Longitudinal-mode natural frequencies are insensitive to the operating speed. The degenerate zero-speed bending-mode natural frequencies split into distinct ones as the operating speed increases.
(ii) Both disk flexibility and boundary conditions affect the natural frequencies of the system and consequently vibratory behaviour, as well as critical speeds, are also affected. The disk flexibility introduces supplementary modes and gives account of disk modes. The fixed boundary condition makes the system more rigid, contrary to the case involving an elastic bearing.

In a future work, we will be interested in the study of the dynamic behaviour of a spinning shaft–disk system in the presence of geometrical defects. We will develop a mathematical model that is able to describe these defects.

References

1. Chivens DR, Nelson HD (1975) The natural frequencies and critical speeds of a rotating flexible shaft–disk–spindle system. ASME J Eng Indus 96:1328–1333
2. Flowers GT, Ryan SG (1993) Development of a set of equations for incorporating disk flexibility effects in rotor-dynamic analyses. ASME J Eng Gas Turb Power 115:227–233
3. Flowers GT, Wu F (1996) Disk–shaft vibration induced by bearing clearance effects: analysis and experiment. ASME J Eng Gas Turb Power 118:204–208
4. Jang GH, Lee SH, Jung MS (2002) Free vibration analysis of a spinning flexible disk–spindle system supported by ball bearing and flexible shaft using the finite element method and substructure synthesis. J Sound Vibr 251:59–78
5. Lee CW (1997) Prediction of coupled vibrations in hard disk drive spindle system. Proc ASME 16th Biennial Conf Vibr Noise
6. Lim S (2000) Finite element analysis of flexural vibrations in hard disk drive spindle systems. J Sound Vibr 233:601–616
7. Parker RG (1999) Analytical vibration of spinning elastic disk spindle systems. ASME J Appl Mech 66:218–224
8. Parker RG, Sathe PJ (1999) Free vibration and stability of spinning disk–spindle system. ASME J Vibr Acoust 121:393–396
9. Shen IY, Ku C-PR (1997) A nonclassical vibration analysis of a multiple rotating disk and spindle assembly. J Appl Mech 64:165–174
10. Batoz J-L, Gouri D (1990) Modélisation des Structures par Éléments Finis. Paris Editions Hermès
11. Lin J, Parker RG (1999) Sensitivity of planetary gear natural frequencies and vibration modes to model parameters. J Sound Vibr 228:109–128
12. Lalanne M, Ferraris G (1996) Dynamique des Rotors en Flexion. Techniques de l'ingénieur, traité Génie mécanique